

Intercalation-Based Single-Molecule Fluorescence Assay To Study DNA Supercoil Dynamics

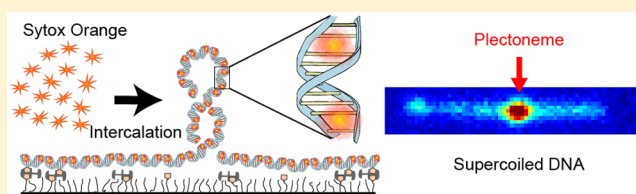
Mahipal Ganji, Sung Hyun Kim, Jaco van der Torre, Elio Abbondanzieri,* and Cees Dekker*

Department of Bionanoscience, Kavli Institute of Nanoscience, Delft University of Technology, Van der Maasweg 9, Delft, 2629HZ, The Netherlands

Supporting Information

ABSTRACT: DNA supercoiling crucially affects cellular processes such as DNA replication, gene expression, and chromatin organization. However, mechanistic understanding of DNA supercoiling and the related DNA-processing enzymes has remained limited, mainly due to the lack of convenient experimental tools to probe these phenomena. Here, we report a novel high-throughput single-molecule assay for real-time visualization of supercoiled DNA molecules, named ISD (Intercalation-induced Supercoiling of DNA). We use an intercalating dye to induce supercoiling of surface-attached DNA molecules as well as to visualize coiled-loop structures (i.e., plectonemes) formed on DNA. The technique is solely based on epifluorescence microscopy and requires no mechanical manipulation of the DNA molecules. This new assay allows to track positions and sizes of individual plectonemes and characterize their position-dependent dynamics such as nucleation, termination, and diffusion. We describe the ISD technique and demonstrate its potential by establishing that plectonemes are pinned to a local 10-nucleotide long mispaired sequence along a double-stranded DNA molecule.

KEYWORDS: single-molecule, DNA supercoiling, plectoneme, fluorescence, intercalation



DNA supercoiling plays a vital role in most cellular processes including DNA replication and gene expression.^{1–6} Failure to control the degree of supercoiling can be lethal.⁷ Indeed, the supercoiling state of genomic DNA is precisely controlled over the course of the cell cycle and is subject to change in response to environmental factors such as temperature jumps or starvation.^{8,9} Electron-microscopy studies revealed that the *Escherichia coli* genome is organized into 50–100 topological domains with a length of 20–100 kilobase pairs (kbp), where each domain allows for independent control of the degree of supercoiling of its DNA segment.^{10,11} Most regions of the DNA are maintained in a negatively supercoiled state for easier access of the DNA bases to proteins, but positively supercoiled domains are also present.¹² Interestingly, thermophilic bacterial species keep most DNA in a positively supercoiled state to avoid excessive denaturation of DNA at the high temperature of their environment.^{13,14}

Supercoiling induces significant alterations in the three-dimensional structure of DNA. For example, the formation of a type of DNA supercoil called plectonemes, where the DNA helix is coiled onto itself (cf. Figure 1D), brings distant DNA segments in close proximity, which subsequently alters the activity of DNA-processing proteins such as transcription-regulatory proteins or site-specific recombinases.^{15–19} These enzymatic activities in turn can change the supercoiling state of DNA transiently or permanently.^{5,20} Also, local defects in the B-form DNA structure such as kinks or bubbles have been theorized to affect the locations of plectonemes.²¹

Despite the ubiquitous importance of DNA supercoiling, a mechanistic understanding of the role of supercoiled DNA in various cellular processes has remained limited. This is mainly due to the lack of a convenient experimental platform that allows real-time in situ visualization of the DNA structure under different degrees of supercoiling. Indirect measurements, such as biochemical assays of enzymatic activity on supercoiled DNA, hardly allow for an unambiguous interpretation of the DNA structure. And direct measurements of DNA structure using electron-microscopy and atomic-force microscopy only provide static images of DNA plasmids with limited control of the supercoiling state.^{22–30} Force-spectroscopy techniques such as magnetic tweezers and optical torque wrenches have been developed for mechanical measurements on supercoiled DNA with precise control of the tension and torque applied.^{31–33} However, most of these single-molecule techniques merely measure the end-to-end extension of the DNA, which provides only limited structural information. Real-time visualization of the dynamics of plectonemes within a single DNA molecule has only recently been achieved by combining fluorescence microscopy and magnetic tweezers in a side-pulling geometry.³⁴ This technique provided a powerful demonstration of the feasibility to visualize and study the DNA supercoiling, but the fairly complicated instrumentation and sample preparation and

Received: June 1, 2016

Revised: June 27, 2016

Published: June 29, 2016

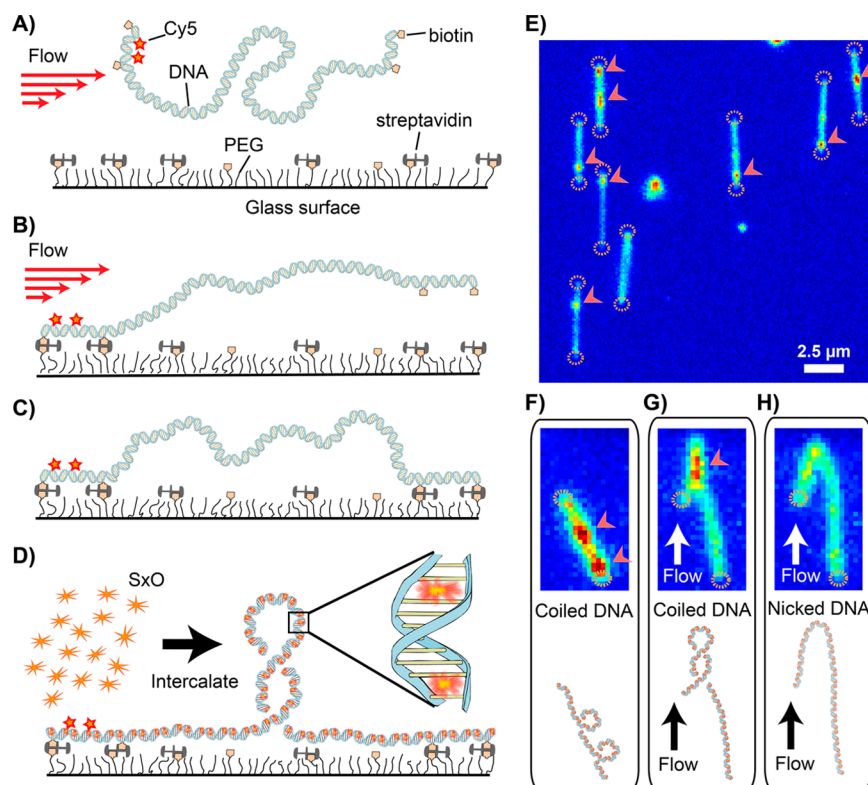


Figure 1. Visualization of supercoiled DNA induced by intercalating dyes. (A–D) Schematics of the preparation of doubly tethered, supercoiled DNA. (A) Biotinylated-DNA is applied under flow to a surface containing immobilized biotin–streptavidin complexes. Cy5 (red star) fluorophores identify the DNA orientation. (B) One of the DNA ends binds to the surface causing the DNA molecule to be stretched by the flow. (C) Binding of the remaining DNA end locks the molecule in an extended conformation. Multiple streptavidin–biotin links at each DNA end ensure the DNA is torsionally constrained. (D) Binding of the intercalating Sytox orange dyes (SxO, orange stars) unwinds the DNA and generates torsional stress that lead to plectonemes in the DNA. (E) Example of a fluorescence image of SxO stained DNA obtained with the epifluorescence microscope. Among the eight stretched DNA molecules in the field of view, seven showed plectonemes (indicated by arrows). Dashed circles represent DNA anchor points. (F) Image of a single DNA molecule with multiple plectonemes (red arrows) observed without flow. A schematic of the DNA molecule is drawn at the bottom for visual guide. (G) Visualization of the same DNA molecule under flow shows a single plectoneme (red arrow) stretched in the direction of flow. (H) After photoinduced nicking, the plectonemes vanish and the DNA adopts a J-shaped structure under flow.

the low throughput of the method have prevented it from becoming widely accessible.

Here, we report a novel high-throughput single-molecule assay to control and visualize DNA supercoils using only a conventional fluorescence microscope. We use intercalating dyes to induce supercoils within a linear DNA molecule that is bound to a surface at its two ends in such a way that it is torsionally constrained. Intercalation of dye molecules between the DNA bases results in a local change of the rise and twist of the B-form DNA,^{35–37} which globally induces twist to the DNA molecule.³⁸ Indeed, we show that this simple approach makes it possible to precisely control the degree of supercoiling of the DNA by changing the concentration of the intercalating dye. Therefore, there is no need for direct mechanical manipulation on the DNA, which requires a more complicated experimental measurement apparatus.³⁴ Moreover, visualization of the plectonemes that are induced by the coiling of the DNA is directly accessible by measuring the fluorescence intensity of the intercalating dye. We name this new assay Intercalation-induced Supercoiling of DNA (ISD). Using this assay, we measured the size and position of individual plectonemes along DNA to characterize their position-dependent dynamics such as nucleation, termination, and diffusion. We then applied this new assay to study a pinning effect of plectonemes at a local single-stranded region of mismatched bases.

To visualize supercoiled DNA (Figure 1), we prepared 20 kbp-long linear DNA with multiple biotins labeled at its end regions (~500 bp at each of the ends). To determine the direction of each DNA molecule, we further labeled one of the DNA ends with Cy5, which can be identified under 640 nm laser illumination (Supporting Information, Figure S1). We flowed the DNA molecules into a microfluidic channel in which the surface is coated with streptavidin (Figure 1A and Figure S1A). Under constant flow, one end of the DNA molecule first binds to the surface, causing the DNA molecule to be linearly stretched along the flow (Figure 1B). Subsequently, the other end of the DNA binds to the surface (Figure 1C).^{39,40} We set the flow rate to obtain a DNA extension of around 65–70% of its B-form contour length (Figure S2A). Unbound DNA molecules were washed off before the injection of a buffer containing 30 nM of the intercalating dye Sytox Orange (SxO). We chose the monomeric cyanine nucleic-acid stain SxO for inducing and visualizing DNA supercoils for a number of reasons: First, the high fluorescence quantum yield of the dye ($\Phi = 0.9$) provides a high signal-to-noise-ratio in imaging at our 532 nm excitation. Second, SxO has relatively high binding and dissociation rates⁴¹ which ensures that equilibrium is achieved immediately after buffer exchange and which also minimizes the number of photobleached dye molecules bound to DNA (as those will disassociate and get replaced). Third, the dye exhibits

a more than 500-fold fluorescence enhancement upon binding to DNA, minimizing the fluorescence background from the free dyes in the solution. Upon flushing the buffer containing SxO into the flow cell, dye molecules bind to DNA by intercalating between bases, resulting in local unwinding of helical structure. Because each end of the DNA has multiple biotin–streptavidin linkages, the torsional stress induced by the intercalation of the dye molecules is not relaxed and instead accumulates to induce positive supercoiling in the form of plectonemes (Figure 1D).

We employed dual-color epifluorescence microscopy in order to visualize the tethered DNA molecule and the plectonemes induced in it (Figure S1). Shown in the Figure 1E is a representative fluorescence image with eight stretched DNA molecules. Note that the DNA molecules display a homogeneous fluorescence intensity with additional bright fluorescent local spots, which are consistent with the formation of local plectonemes (Figure 1E–G, red arrows) [cf. the very similar images in a previous report of DNA supercoils].³⁴ These spots disappeared suddenly and irreversibly over time under prolonged laser illumination, presumably because of the photoinduced appearance of a local nick along the DNA molecule. After the photoinduced nicking, the intensity profile of the DNA molecule became very homogeneous along the length of the DNA, showing no detectable sequence-dependence in the binding of SxO dye (Figure S2B). Note that these fluorescent spots display the exact same behavior as the local plectonemes observed with side-pulling magnetic tweezers.³⁴ To further confirm that the observed spots were indeed plectonemes, we performed two additional experiments. First, we visualized DNA molecules which were pretreated with a nicking enzyme. As expected, we did not observe any bright spots on these nicked DNA molecules. Second, we directly visualized plectonemes emerging from DNA exhibiting bright spots using flow stretching. We selected a DNA molecule which was not oriented parallel to the direction of flow (Figure 1E–G and Movie S1). Before applying flow, the molecule was linear and showed the characteristic bright spots (Figure 1F). During the flow, under an oblique angle, a branch in the DNA molecule emerged in the direction of flow (Figure 1G), resulting in a Y-shaped molecule. The downstream-flow-aligned branch of the DNA exhibited a higher fluorescence intensity compared to the other branches, indicating this branch was a plectoneme containing two DNA strands wound around each other. After prolonged exposure to the excitation light, the plectonemic region suddenly unwound, likely due to photoinduced nicking of the DNA, creating a J-shaped DNA molecule with a uniform intensity (Figure 1H). These observations confirm that the bright fluorescent spots that we observed were indeed DNA plectonemes.

Having established that SxO can be used to form plectonemes, we next used magnetic tweezers⁴² to examine if the intercalation of SxO dyes modifies the mechanical properties of DNA. We prepared DNA molecules identical to those used above except that the biotin labels at the Cy5-end were replaced with digoxigenin. We then tethered the digoxigenin-labeled ends of the DNA molecules to a glass surface coated with antidigoxigenin and attached the biotin-labeled DNA ends to magnetic beads coated with streptavidin. Then, by using a pair of magnets, we observed the mechanical response of the DNA molecules under a range of tensions and torques in the presence of SxO.

We first examined the end-to-end length change of a torsionally unconstrained (i.e., nicked) DNA at different applied forces in the presence or absence of SxO (Figure 2A). Force–extension curves from torsionally unconstrained

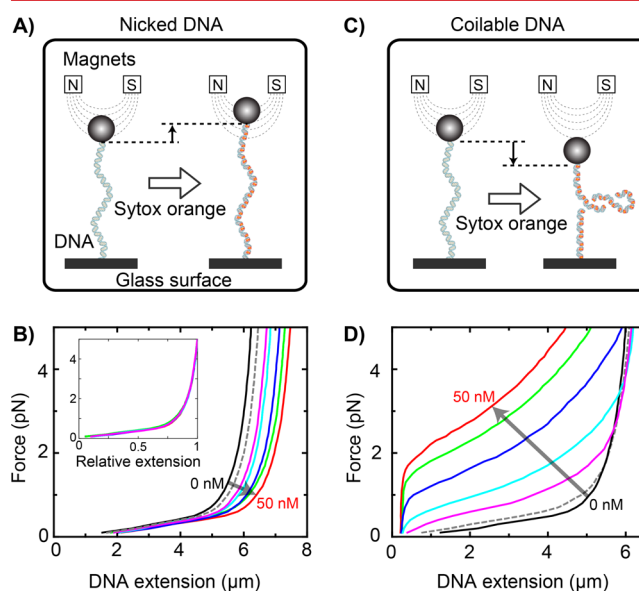


Figure 2. DNA force–extension curves from single-molecule magnetic tweezers assay. (A) Schematic diagram showing lengthening of nicked DNA molecule, held in magnetic field created by a pair of magnets, upon binding of SxO. (B) Force–extension curves of nicked DNA measured at various SxO concentrations (black, pink, cyan, blue, green, and red: 0, 5, 10, 15, 30, and 50 nM). The dotted gray curve was obtained after washing off 50 nM SxO with SxO free buffer. Inset shows the same DNA extension curves normalized to their maximum length. (C) Schematic diagram shows the intercalating dye-induced plectoneme formation on torsionally constrained DNA, resulting in the decrease in the DNA extension. (D) Force–extension curves of the torsionally constrained DNA (color scheme for the SxO concentrations is the same as in (B)).

DNA are shown in Figure 2B. In the force range of 1–5 pN, we observed an increase in the end-to-end distance of the DNA as we increased the concentration of SxO. For example, at 3 pN force and 30 nM SxO, we observed 21% increase in the DNA extension. Importantly, upon normalizing the end-to-end length of the DNA with its maximum length at 5 pN, the force–extension curves of the DNA for all SxO concentrations overlapped with each other (Figure 2B, inset), implying that the intercalation of the dye did not significantly alter the mechanical properties of the DNA other than slightly extending the contour length. When we flushed out the flow cell with a SxO-free buffer, the force–extension curve nearly reverted back to that of the bare DNA, confirming that the dye binding is reversible (Figure 2B, gray dashed line).

We also measured force–extension curves for torsionally constrained DNA (Figure 2C). In the absence of SxO, no difference was observed between torsionally unconstrained and constrained DNA, indicating the DNA was initially torsionally relaxed (Figure 2B,D, black curves). However, upon addition of SxO, the torsionally constrained DNA exhibited a different behavior (Figure 2D) compared to the torsionally unconstrained DNA (Figure 2B). As we increased the concentration of SxO, the end-to-end extension of the torsionally constrained DNA systematically decreased due to the formation of

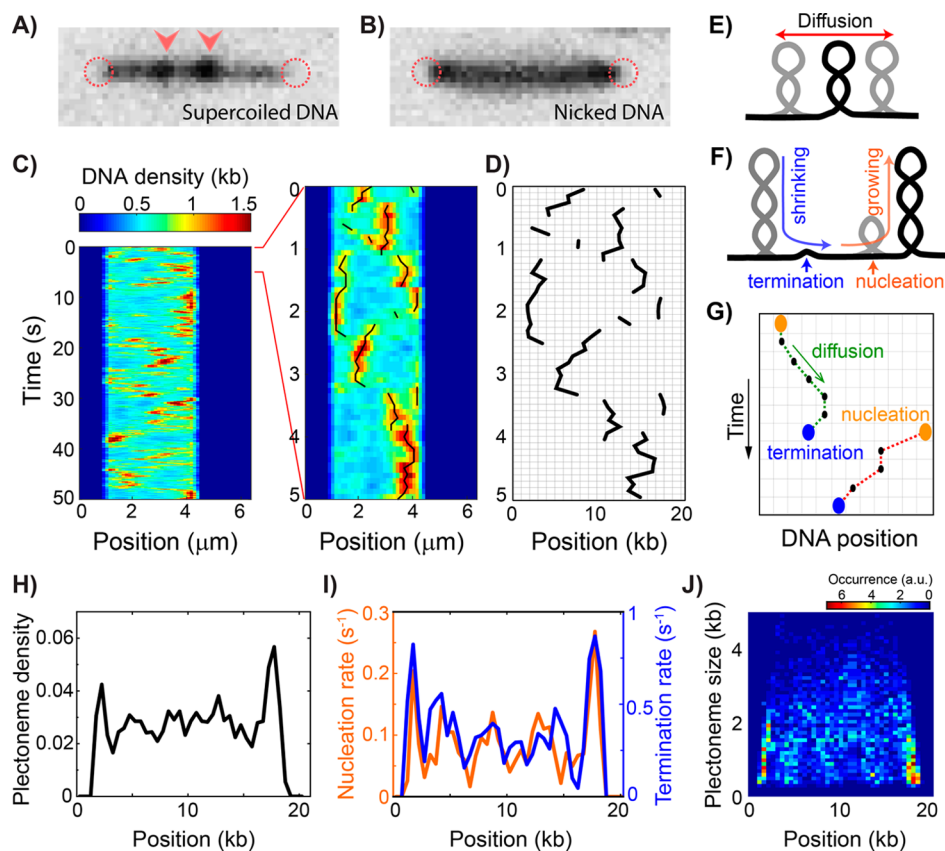


Figure 3. Real-time observation of DNA plectoneme dynamics. (A) Fluorescence image of a supercoiled DNA with multiple plectonemes (red arrows). Dotted circles indicate DNA anchoring positions on surface (B) Fluorescence intensity image of the same molecule as in (A) after nicking. (C) Representative DNA density kymograph of a supercoiled DNA molecule. Close up view of the first 5 s is shown in the right panel. Overlaid black curves show the positions of individual plectonemes identified by a threshold algorithm. (D) Plectoneme positions are plotted in DNA base pair space (i.e., in the unit of kbp). (E) Schematic diagram showing the diffusion of a plectoneme. (F) Diagram showing the nucleation and termination processes coupled with the plectoneme growth and shrinkage. (G) Schematic DNA plectoneme kymograph showing nucleation, diffusion, and termination of plectonemes. Two plectonemes (green and red) are presented. Presence of plectoneme was represented with dots. Nucleation and termination events were shown with orange and blue dots, respectively. (H–I) The measured plectoneme density (H), the nucleation and termination rates (I), and the position-dependent plectoneme size distributions from the single DNA molecule presented in (C).

plectonemes. This empirical force–extension relationship measured with magnetic tweezers also allows to estimate the tension within the DNA in ISD measurements (Figure S2A). We then measured the extension-rotation curves of DNA molecules at 3 pN under different SxO concentrations (Figure S2C). When we unwound the torsionally constrained DNA, the end-to-end length linearly increased until it reached to a plateau where all the dye-induced plectonemes were relaxed. Importantly, the slopes within the linearly increasing regions of the rotation curves (i.e., on the right side of Figure S2C) remained the same regardless of the SxO concentration, implying that the size and curvature of the loops in plectonemes did not change significantly upon binding of SxO in our buffer conditions. From the measured rotation curves, we estimate the number of coils (writhing number) put in plectonemic DNA due to binding of SxO. For instance, at a DNA stretching of 3 pN with 30 nM SxO concentration the number of turns induced into the DNA was 31. Thus, by using force–rotation curves from single-molecule magnetic tweezers as reference, we are able to estimate the number of coils applied on each DNA molecule in our ISD assay.

Having successfully characterized the degree of dye-induced supercoiling, we return to the ISD assay to investigate the dynamics of individual plectonemes. We recorded fluorescence

movies of the DNA dynamics with 100 ms exposure time per frame (Figure 3A). The fluorescence images of the same DNA molecules were also measured after photoinduced nicking of the DNA to confirm that the plectonemes disappeared (Figure 3B). We extracted fluorescence intensity profiles along individual DNA molecules for every frame to build intensity kymographs (Figure S3A,B). For quantitative analysis, the fluorescence intensity was converted to DNA density by mapping the intensity profiles of the supercoiled DNA onto the intensity profile of the corresponding torsionally relaxed molecule (see Figure S3C–E, and Materials and Methods for detail). A characteristic example of the converted DNA density kymograph is shown in Figure 3C.

Next, we applied a threshold algorithm to the DNA density kymograph to track the position and size of individual plectonemes (Figure 3D and Figure S3F). Plectonemes appearing in consecutive frames were considered to be continuous if they appeared within 3 pixels (~ 360 nm or ~ 1 kbp) of each other. In order to reduce false positives due to noise, we only included plectonemes that were present for at least two consecutive frames. In this way, diffusing plectonemes (Figure 3E) could be tracked over time. If plectonemes in consecutive frames were separated by more than 3 pixels, we assumed that the existing plectoneme terminated and a new

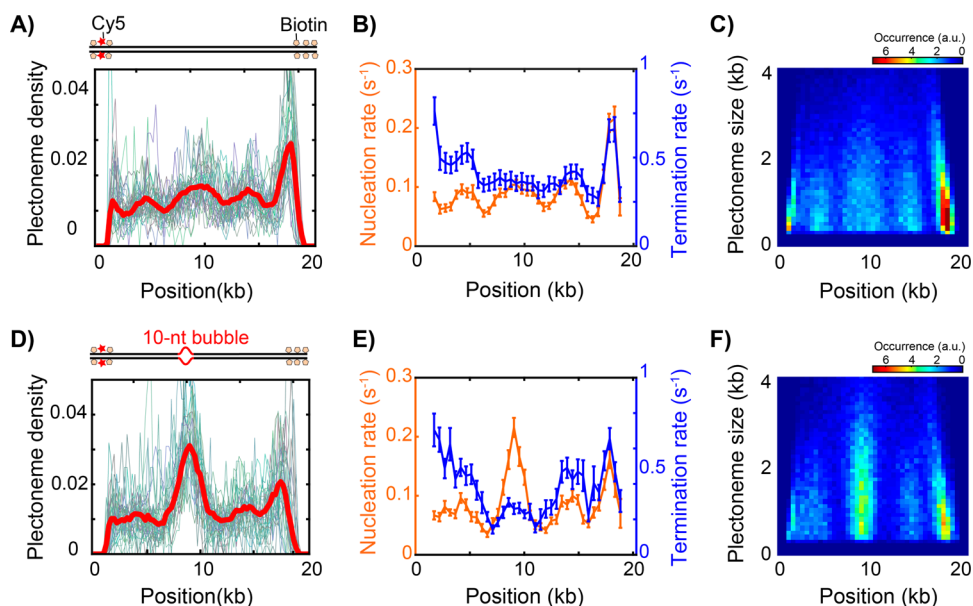


Figure 4. DNA sequence-dependent pinning of plectonemes. (A) Plectoneme densities of 46 identical DNA molecules (thin lines) and their average (red thick line). The schematic of the DNA construct is shown above (red star and orange pentagons represent Cy5 and biotin, respectively). (B) Averaged nucleation (orange) and termination (blue) rates observed. (Error bars are sem.) (C) Averaged position-dependent plectoneme size distributions. (D) Plectoneme densities of 47 identical DNA molecules (thin lines) that contain a local 10-nt mismatched sequence located at 8.8 kbp away from the Cy5 labeled end as illustrated in the top panel. Red thick line is the averaged plectoneme density of the individuals. (E) Averaged nucleation (orange) and termination (blue) rates observed for the 10-nt mismatched sequence. (F) Averaged position-dependent plectoneme size distributions of the 10-nt mismatched sequences.

plectoneme had nucleated at a different position (Figure 3F). We marked the position of first appearance of each plectoneme as the nucleation point and the last position as the terminating point (Figure 3G). In Figure 3C (right panel), we plotted the tracked position of the individual plectonemes on the DNA density kymograph. Note that the trajectories of the plectonemes in Figure 3D were plotted as a function of the genomic position along the DNA (i.e., in units of kbp). We also obtained the mean-square-displacement (MSD) of plectonemes from the individual time-trajectories of plectoneme displacement, to yield a diffusion coefficient $D = 4.8 \text{ kbp}^2/\text{s}$ ($0.13 \mu\text{m}^2/\text{s}$), from the slope of the MSD versus time (Figure S4). The size of individual plectonemes was determined from the fluorescence intensity by summing up the excess amount of DNA above the average DNA density in a local region.

On the basis of the determined position and size of individual plectonemes, we constructed a probability density function for the plectonemes, hereafter referred to as the plectoneme density, versus the genomic position along the DNA. The plectoneme density was obtained by building a normalized histogram of the genomic positions of individual plectonemes collected from all time frames (Figure 3H, see Materials and Methods for details). We also counted the total number of nucleation and termination events at each position of the DNA to obtain position-dependent nucleation and termination rates (Figure 3I). The observed size of plectonemes varied between 150 bp to 4 kbp (Figure 3J), in good agreement with our previous study.³⁴

Interestingly, the observed plectoneme density and the nucleation and termination rates showed position-dependent variations (Figure 3G–J). As inhomogeneity in the formation of plectonemes could be due to the particular molecule, we measured many ($N = 46$) identical DNA molecules and averaged the results (see Figure 4A–C). The inhomogeneity

was still observed in the averages of the plectoneme density (Figure 4A, thick red line), the nucleation and termination rates (Figure 4B), and the position-dependent plectoneme size distribution (Figure 4C). Similarly, dynamical properties of plectoneme such as the lifetime and local diffusion constant were observed to be position dependent (Figure S5). This demonstrates that the plectoneme properties reflect features encoded within the DNA sequence.⁴³ Interestingly, we observed a strong peak near one end of the DNA (at ~ 18 kbp) in the plectoneme density, nucleation and termination rates, and plectoneme size distributions (Figure 4A–C). Because there was no such a peak at the other end of the DNA, the strong peak was likely not an artifact of the DNA–surface linkage and instead reflects some property of the local sequence. Interestingly, when we measured the plectonemes formed on negatively supercoiled DNA molecules (see Materials and Methods for the details of preparation), we obtained somewhat different patterns in the plectoneme density and the nucleation and termination rates (Figure S6). While the current paper reports the new methodology to observe DNA supercoils, this sequence dependence is of obvious importance and will be studied in full detail in future work.

In cells, DNA plectonemes can potentially pin their position to local structures such as DNA-bound proteins or defects in the DNA. We used the new ISD technique to address one such example. As nucleation of a plectoneme requires a large bending of a local region of DNA, a locally flexible DNA region would significantly promote the preferential formation and growth of a plectoneme at this particular site as it would require less energy to bend the DNA into the tip of a plectoneme.⁴⁴ To examine if a flexible DNA region indeed serves as a nucleation site that localizes a plectoneme, we inserted a 10-nucleotide mismatched sequence (i.e., a local region where the sequences of both strands do not allow base pairing) at a position 8.8-kbp

away from the Cy5-end of the DNA (Figure 4D). The measured plectoneme density then showed a pronounced peak at the position of this mismatch sequence, confirming that the flexible DNA bubble pins plectonemes at this position. As expected, the plectonemes nucleated more frequently at the mismatch site while the termination rate was lowered at this position (Figure 4E). Plectonemes also grew larger at the mismatch site (Figure 4F and Figure S5G). Furthermore, plectonemes were observed to diffuse toward the mismatch site from both sides and survived longer near the mismatched bubble (Figure S5B and S5F). We observed the same pinning effect by a mispaired bubble using a side-pulling magnetic tweezers assay where the DNA was visualized using covalently attached dyes (Figure S7), as described previously.³⁴ This control measurement rules out that the plectoneme localization observed in Figure 4D–F was an artifact from the intercalation of SxO to DNA. The strong localization effect caused by a DNA mismatch bubble suggests that DNA enzymes that induce local DNA melting, such as RNA polymerase, may also localize a plectonemic structure at the location of the enzyme on the DNA.

Summing up, we have established ISD as a novel high-throughput technique that allows real-time observation of multiple supercoiled DNA molecules simultaneously using a conventional fluorescence microscopy with a simple sample preparation. The first data taken with ISD demonstrates that the visualization of individual plectonemes in a supercoiled DNA can identify sequence-dependent features of the DNA plectoneme dynamics, such as plectoneme pinning by a 10-nucleotide DNA bubble. The throughput of the current assay can be further improved by patterned immobilization of the stretched DNA to visualize hundreds of molecules simultaneously.⁴⁵ Additionally, the current spatial resolution of our fluorescence microscopy is limited by the optical diffraction limit and does not allow to distinguish two plectonemes in close proximity (<350 nm, < 1 kbp). This resolution could be improved by combining ISD with recent advances of super-resolution microscopy such as STED.^{46,47} Furthermore, ISD is capable of detecting other DNA processes such as protein-mediated loop formation and DNA condensation by utilizing multicolor fluorescence imaging, making the technique more broadly applicable to different biological systems. By significantly lowering the barrier for visualizing dynamic plectoneme structures, ISD allows researchers to explore how DNA structure is influenced by DNA sequence and enzymatic activity on supercoiled DNA.

Materials and Methods. Preparation of DNA. DNA molecules were made by using PCR, oligonucleotide hybridization, digestion and DNA ligation (see Supplementary Text 1 and Tables 1 and 2 for detail). Each DNA fragment was digested to the desired length using the restriction enzyme BsaI, which leaves an overhang outside of the recognition site giving us the possibility to specifically ligate different fragments together. The digested DNA fragments were then ligated using T4 DNA ligase (Promega) to make 20 kbp long DNA molecules. For surface immobilization, we further extended the DNA molecules at both ends with 500 bp long DNA fragments containing biotinylated dUTP (biotin-16-dUTP, Roche). We also incorporated aminoallyl-dUTP-Cy5 (Jena Bioscience) to one of the biotin-DNA fragments to distinguish between the different ends. The desired DNA molecule was gel purified.

Dual-Color Epifluorescence Microscopy. A schematic of the custom-made epifluorescence microscopy setup is shown in

Figure S1. We combined two lasers (532 nm Cobolt Samba and 640 nm Cobolt MLD, Cobolt AB) using a dichroic mirror and sent them through an acousto-optic tunable filter (AOTF, AA Opto electronic) for a programmable switching of the two lasers lines. The lasers were then focused at the back-focal plane of an objective lens (60× UPLSAPO, NA 1.2, water immersion, Olympus) for the wide-field, epifluorescence-mode illumination. Fluorescence emission from the sample was collected by the same objective lens and separated from the laser beams by using a dichroic mirror (Di01-R405/488/543/635, Semrock). The fluorescence signal was focused by a lens ($f_1 = 50$ mm) and spatially filtered by passing through a slit. The fluorescence was then collimated again by using another lens ($f_2 = 100$ mm) before the spectral separation of SxO and Cy5 by a dichroic mirror (FF635-Di02, Semrock). Band pass filters at 731/137 nm (FF01-731/137, Semrock) and 571/72 nm (FF01-571/72, Semrock) were employed to avoid cross talk between the channels. Additionally, a 550 nm long pass filter (FEL0550, Thorlabs) was placed in the SxO emission path to eliminate the back scattered 532 nm laser light. Finally, two lenses ($f = 200$ mm) and a dichroic mirror (FF635-Di02, Semrock) were used to combine and image the fluorescence signals onto an EMCCD camera (Ixon 897, Andor). The AOTF and the EMCCD was synchronized for the alternative laser excitation by using a PCIe-6320 card and a BNC-2120 breakout box (National Instruments) and controlled by a home-built LabVIEW software. The EMCCD was operated at -90 °C and at an em-gain of 1000 for data acquisition.

Intercalation-Induced Supercoiling of DNA (ISD). A flow cell for DNA immobilization and buffer exchange was prepared by sandwiching a quartz slide and a glass coverslip with double-sided tape. Holes in the quartz slide serves as an inlet and outlet for buffer exchange (Figure S1B). Typically, a flow channel holds 10 μ L of solution. The inner surface of the flow channel were passivated with polyethylene glycol (PEG) to suppress nonspecific binding of SxO and 2% (w/w) of the PEG molecules were functionalized with biotin so that the biotinylated DNA could be immobilized on the surface via biotin–streptavidin linkage.⁴⁸

For immobilization of DNA, we first flowed 20 μ L of 0.1 mg/mL streptavidin into a flow cell and incubated for 1 min. After washing excess streptavidin that did not bind to the surface, we introduced 30 μ L of 1–10 pM of biotinylated-DNA molecules at a flow rate of 50 μ L/min (Figure 1A). Immediately after the flow, we further flowed 200 μ L of a washing buffer (40 mM Tris–HCl, pH 8.0, 20 mM NaCl, 0.4 mM EDTA) at the same flow rate to ensure stretching and tethering of the other end of the DNA to the surface (Figure 1C). We typically obtained a stretch of around 60–65% of the contour length of the B-form DNA (Figure S2A).

To induce supercoiling of the tethered DNA, we flowed in 30 nM Sytox orange (S11368, Thermo Fisher) in an imaging buffer consisting of 40 mM Tris–HCl, pH 8.0, 20 mM NaCl, and 0.4 mM EDTA. We also included an oxygen scavenging system consisting of 2 mM Trolox, 40 μ g/mL glucose oxidase, 17 μ g/mL catalase, and 5% (wt/v) D-dextrose in the imaging buffer for minimization of photobleaching of the fluorophores.

To prepare negatively supercoiled DNA, we first immobilized DNA to the surface in the presence of high concentration of SxO (150 nM), and subsequently reduced the dye concentration to 30 nM for the measurements. The subsequent release of prebound SxO dyes after immobilization of the DNA results in negative supercoiling of the DNA.

Magnetic Tweezers. The magnetic tweezers apparatus is similar to the one reported previously.⁴⁹ A flow cell was prepared by sandwiching two polystyrene-coated coverslips with a parafilm as a spacer. The flow cell was then incubated with 1 mg/mL antidigoxigenin in a buffer carrying 20 mM Tris-HCl, pH 8.0, 20 mM NaCl, and 5 mM EDTA for 15 min. Alongside, streptavidin-coated magnetic beads (2.8 μm diameter, M270, Thermo Fisher) were washed with buffer A (20 mM TrisHCl pH8.0, 200 mM NaCl, 5 mM EDTA, 0.25% (v/v) Tween20) and incubated with the 21 kbp DNA functionalized with biotin at one end and digoxigenin at the other end for 15 min. After incubation, unbound DNA was washed with buffer A and the mixture was flowed into the flow cell and incubated for 15 min for surface immobilization. The flow cell was washed with excess amount of buffer A until all the unbound beads were removed. After the washing, we introduced the same measurement buffer, which we used for the fluorescence measurement with indicated concentration of SxO to record force–extension curves of DNA. The force–extension curves were measured by approaching the magnet to the DNA tethered surface at a speed of 0.1 pN/s.

Side-Pulling Magnetic Tweezers Combined with Fluorescence Microscopy. The details of the side-pulling magnetic tweezers assay are described in our previous report.³⁴ Briefly, a 20 kbp long DNA functionalized with biotin and digoxigenin at each end was labeled with Cy3 using a commercial nucleic acid labeling reagent (Label IT, MIR3625, Mirus Bio).⁵⁰ The labeled DNA was incubated with a streptavidin-coated magnetic beads (1 μm , New England Biolabs) in buffer A for 15 min. The bead/DNA mixture was washed and reconstituted in buffer A to remove unbound DNA molecules and flowed in a square-hollowed glass capillary (8270, VitroCom) pretreated with polystyrene (0.1% in toluene, brief immersing) and antidigoxigenin (1 mg/mL, 15 min incubation). After 15 min incubation of the bead/DNA mixture, the capillary was washed with excess amount of buffer A to remove unbound bead/DNA. Then a imaging buffer carrying 20 mM TrisHCl pH 7.5, 2.5 mM dihydroxybenzoic acid, 50 nM protocatechuate 3,4-dioxygenase, 1 mM Trolox, 100 μM *n*-propyl gallate, and 0.1% (v/v) Tween20.

The side-pulling magnetic tweezers setup combined with epifluorescence microscopy was built around an inverted microscope (Axiovert 200M, Zeiss) equipped with a 532 nm Laser (Sapphire, Coherent) and a scientific-grade CMOS camera (Neo, Andor).³⁴ The surface immobilized DNA was first stretched upward by placing a pair of magnet on top of the capillary to apply rotations to the magnetic bead. After applying a desired number of rotations, the bead was pulled from the side by approaching another magnet horizontally, followed by removal of the top magnets. The tension applied to the DNA was calibrated by measuring the power spectrum of the position fluctuation of the bead.⁵¹ The fluorescence from the labeled DNA were collected by an objective lens (NA1.4, 63 \times , Oil immersion, Plan-Apochromat, Zeiss) and filtered through a bandpass filter (FF01-585/40, Semrock) to remove back scattered laser light. Images were acquired with 20 ms exposure time.

Image Analysis. Fluorescence images were analyzed using custom written software in Matlab (Mathworks, available upon request). The first 10 frames of the measured fluorescence images were averaged and used to determine the end position of individual DNA molecules. After selection of a molecule, the images with 640 nm illumination at the same field of view were

loaded and used to identify the direction of the DNA molecule. Then, fluorescence intensity profiles of the DNA along its longitudinal direction were calculated by summing up the intensities from 11 nearby pixels that lay perpendicular to the DNA at each position. The background intensity of the image was determined by taking the median value of the pixels around the DNA. The background intensity was subtracted from the intensity profile which was then normalized to compensate for photobleaching of SxO. After analyzing all the frames, the normalized intensity profiles were aligned to build an intensity kymograph (Figure S3C).

DNA Density Estimation from Fluorescence Intensity. Although peaks in the intensity profile indicate the position of individual plectonemes in real space, it cannot be read as the position in the base pair space because of the nonlinearity caused by presence of other plectonemes, which put more DNA into certain pixels (Figure S3B). Moreover, because of the illumination profile and detection efficiency in the field of view is not exactly the same for each pixel, the observed intensity values at each position of the DNA cannot be directly converted to the amount of DNA. To calculate the amount of DNA per pixel (DNA density) in the intensity profiles of the supercoiled DNA, we map it into the intensity profile of the same DNA molecule measured after relaxation of torsional stress due to photoinduced nicking (Figure S3D). We then obtain a kymograph of DNA density (Figure S3E).

Plectoneme Detection and Analysis. A threshold algorithm was applied to the DNA density profile to determine the position and size of individual plectonemes. First, the background DNA density was determined by taking global median value of all the DNA density profiles in a kymograph. Then, the threshold level was set to be 25% above the background DNA density (Figure S3F). Among the peaks detected above the threshold, only those that were observed longer than two consecutive time frames were selected as plectoneme. The size of the plectoneme was determined by summing up 5 pixels around each peak. If a plectoneme was found more than 3 pixels away in the next time frame, we counted it as nucleation of new plectoneme at that pixel and simultaneously termination of the plectoneme in the previous time frame (Figure 3F). The threshold algorithm applied to the DNA density kymograph determined the positions of each plectoneme in real-space, that is, pixel position. The pixel positions of each plectoneme were then converted to the genomic positions (base pair position) by summing up of the DNA densities in the left-side pixels of the plectoneme. Once all the plectonemes were identified, we calculated the probability of finding a plectoneme (plectoneme density) at each position along the DNA in base pair space, by counting the number of frames occupied by plectonemes at each position over time. We also calculated the nucleation (termination) rate by counting the number of nucleation (termination) events divided by the sum of time spent without (with) a plectoneme present at that location before the nucleation (termination) of that plectoneme.

■ ASSOCIATED CONTENT

Supporting Information

The Supporting Information is available free of charge on the ACS Publications website at DOI: 10.1021/acs.nanolett.6b02213.

Preparation of DNA constructs, a schematic of dual-color epi-fluorescence microscope setup, estimation of force on immobilized molecules, estimation of number of coils induced by SxO, fluorescence intensity profile of torsionally relaxed DNA molecules, determination of position and size of plectonemes, displacement and MSD of plectonemes, data of plectoneme movement, position-dependent diffusion coefficient, average lifetimes without and with 10-nucleotide mismatch sequence, distribution of plectoneme size at the mismatched position, data of plectonemes on negatively supercoiled DNA molecules, and plectoneme formation and dynamics data from side-pulling magnetic tweezers combined with fluorescence microscopy. (PDF)

Movie showing plectoneme. (AVI)

AUTHOR INFORMATION

Corresponding Authors

*E-mail: c.dekker@tudelft.nl.

*E-mail: e.a.abbondanzieri@tudelft.nl.

Author Contributions

(M. G. and S. H. K.) Equal contributors.

Notes

The authors declare no competing financial interest.

ACKNOWLEDGMENTS

We thank Dr. Jacob W. J. Kerssemakers for contribution in data analysis and insightful discussion. This work was supported by the ERC Advanced Grant SynDiv [grant number 669598 to C.D.]; The Netherlands Organization for Scientific Research (NWO/OCW) [as part of the Frontiers of Nanoscience program], and the ERC Marie Curie Career Integration Grant [grant number 304284].

REFERENCES

- Wang, J. C. *Annu. Rev. Biochem.* **1985**, *54* (1), 665–697.
- Liu, L. F.; Wang, J. C. *Proc. Natl. Acad. Sci. U. S. A.* **1987**, *84* (20), 7024–7027.
- Hatfield, G. W.; Benham, C. J. *Annu. Rev. Genet.* **2002**, *36* (1), 175–203.
- Sherratt, D. J. *Science* **2003**, *301* (5634), 780–785.
- Chong, S.; Chen, C.; Ge, H.; Xie, X. S. *Cell* **2014**, *158* (2), 314–326.
- Roca, J. *Chromosoma* **2011**, *120* (4), 323–334.
- Zechiedrich, E. L.; Khodursky, A. B.; Cozzarelli, N. R. *Genes Dev.* **1997**, *11* (19), 2580–2592.
- Goldstein, E.; Drlica, K. *Proc. Natl. Acad. Sci. U. S. A.* **1984**, *81* (13), 4046–4050.
- Dorman, C. J. *Trends Microbiol.* **1996**, *4* (6), 214–6.
- Kavenoff, R.; Ryder, O. *Chromosoma* **1976**, *55*, 13.
- Postow, L.; Hardy, C. D.; Arsuaga, J.; Cozzarelli, N. R. *Genes Dev.* **2004**, *18* (14), 1766–1779.
- Naughton, C.; Avlonitis, N.; Corless, S.; Prendergast, J. G.; Mati, I. K.; Eijk, P. P.; Cockroft, S. L.; Bradley, M.; Ylstra, B.; Gilbert, N. *Nat. Struct. Mol. Biol.* **2013**, *20* (3), 387–395.
- Perugino, G.; Valenti, A.; D'Amato, A.; Rossi, M.; Ciaramella, M. *Biochem. Soc. Trans.* **2009**, *37* (1), 69–73.
- Forterre, P.; Bergerat, A.; Lopex-Garcia, P. *FEMS Microbiol. Rev.* **1996**, *18* (2–3), 237–248.
- Lavelle, C. *Nat. Struct. Mol. Biol.* **2008**, *15* (2), 123–125.
- Kouzine, F.; Gupta, A.; Baranello, L.; Wojtowicz, D.; Ben-Aissa, K.; Liu, J.; Przytycka, T. M.; Levens, D. *Nat. Struct. Mol. Biol.* **2013**, *20* (3), 396–403.
- Baranello, L.; Levens, D.; Gupta, A.; Kouzine, F. *Biochim. Biophys. Acta, Gene Regul. Mech.* **2012**, *1819* (7), 632–8.
- Kimura, K.; Hirano, T. *Cell* **1997**, *90* (4), 625–634.
- De Vlamincq, I.; Vidic, I.; van Loenhout, M. T. J.; Kanaar, R.; Lebbink, J. H. G.; Dekker, C. *Nucleic Acids Res.* **2010**, *38* (12), 4133–4142.
- Ma, J.; Bai, L.; Wang, M. D. *Science* **2013**, *340* (6140), 1580–1583.
- Brutzer, H.; Luzzietti, N.; Klaue, D.; Seidel, R. *Biophys. J.* **2010**, *98* (7), 1267–1276.
- Lyubchenko, Y. L.; Shlyakhtenko, L. S. *Proc. Natl. Acad. Sci. U. S. A.* **1997**, *94* (2), 496–501.
- Irobalieva, R. N.; Fogg, J. M.; Catanese, D. J.; Sutthibutpong, T.; Chen, M.; Barker, A. K.; Ludtke, S. J.; Harris, S. A.; Schmid, M. F.; Chiu, W.; Zechiedrich, L. *Nat. Commun.* **2015**, *6*, 8440.
- Adrian, M.; ten Heggeler-Bordier, B.; Wahli, W.; Stasiak, A. Z.; Stasiak, A.; Dubochet, J. *EMBO J.* **1990**, *9* (13), 4551–4.
- Amzallag, A.; Vaillant, C.; Jacob, M.; Unser, M.; Bednar, J.; Kahn, J. D.; Dubochet, J.; Stasiak, A.; Maddocks, J. H. *Nucleic Acids Res.* **2006**, *34* (18), e125.
- Bednar, J.; Furrer, P.; Stasiak, A.; Dubochet, J.; Egelman, E. H.; Bates, A. D. *J. Mol. Biol.* **1994**, *235* (3), 825–47.
- Boles, T. C.; White, J. H.; Cozzarelli, N. R. *J. Mol. Biol.* **1990**, *213* (4), 931–951.
- Cherny, D. I.; Jovin, T. M. *J. Mol. Biol.* **2001**, *313* (2), 295–307.
- Levene, S. D.; Donahue, C.; Boles, T. C.; Cozzarelli, N. R. *Biophys. J.* **1995**, *69* (3), 1036–1045.
- Fogg, J. M.; Kolmakova, N.; Rees, I.; Magonov, S.; Hansma, H.; Perona, J. J.; Zechiedrich, E. L. *J. Phys.: Condens. Matter* **2006**, *18* (14), S145–S159.
- La Porta, A.; Wang, M. D. *Phys. Rev. Lett.* **2004**, *92* (19), 190801.
- Strick, T. R.; Allemand, J. F.; Bensimon, D.; Bensimon, A.; Croquette, V. *Science* **1996**, *271* (5257), 1835–7.
- Mosconi, F.; Allemand, J. F.; Bensimon, D.; Croquette, V. *Phys. Rev. Lett.* **2009**, *102* (7), 078301.
- van Loenhout, M. T. J.; de Grunt, M. V.; Dekker, C. *Science* **2012**, *338* (6103), 94–97.
- Gago, F. *Methods* **1998**, *14* (3), 277–292.
- Lee, J. S.; Morgan, A. R. *Nucleic Acids Res.* **1978**, *5* (7), 2425–2439.
- Yao, J.; Lowary, P. T.; Widom, J. *Proc. Natl. Acad. Sci. U. S. A.* **1993**, *90* (20), 9364–8.
- Lipfert, J.; Klijnhout, S.; Dekker, N. H. *Nucleic Acids Res.* **2010**, *38* (20), 7122–32.
- Yardimci, H.; Loveland, A. B.; van Oijen, A. M.; Walter, J. C. *Methods* **2012**, *57* (2), 179–186.
- Graneli, A.; Yeykal, C. C.; Prasad, T. K.; Greene, E. C. *Langmuir* **2006**, *22* (1), 292–9.
- Biebricher, A. S.; Heller, I.; Roijmans, R. F. H.; Hoekstra, T. P.; Peterman, E. J. G.; Wuite, G. J. L. *Nat. Commun.* **2015**, *6*, 7304.
- Strick, T. R.; Allemand, J. F.; Bensimon, D.; Croquette, V. *Biophys. J.* **1998**, *74* (4), 2016–2028.
- Medalion, S.; Rabin, Y. *J. Chem. Phys.* **2016**, *144* (13), 135101.
- Matek, C.; Ouldrige, T. E.; Doye, J. P.; Louis, A. A. *Sci. Rep.* **2015**, *5*, 7655.
- Gorman, J.; Fazio, T.; Wang, F.; Wind, S.; Greene, E. C. *Langmuir* **2010**, *26* (2), 1372–1379.
- Willig, K. I.; Kellner, R. R.; Medda, R.; Hein, B.; Jakobs, S.; Hell, S. W. *Nat. Methods* **2006**, *3* (9), 721–3.
- Heller, I.; Sitters, G.; Broekmans, O. D.; Biebricher, A. S.; Wuite, G. J.; Peterman, E. J. *ChemPhysChem* **2014**, *15* (4), 727–33.
- Chandradoss, S. D.; Haagsma, A. C.; Lee, Y. K.; Hwang, J. H.; Nam, J. M.; Joo, C. *J. Visualized Exp.* **2014**, No. 86, e50549.
- Vlijm, R.; Smitshuijzen, J. S. J.; Lusser, A.; Dekker, C. *PLoS One* **2012**, *7* (9), e46306.
- Slatum, P. S.; Loomis, A. G.; Machnik, K. J.; Watt, M. A.; Duzeski, J. L.; Budker, V. G.; Wolff, J. A.; Hagstrom, J. E. *Mol. Ther.* **2003**, *8* (2), 255–263.

(51) van Loenhout, M. T.; Kerssemakers, J. W.; De Vlaminc, I.; Dekker, C. *Biophys. J.* **2012**, *102* (10), 2362–71.